



# In-Situ Temperature Monitoring and Feedback Control in the Gas Tungsten Arc Welding Process

Anas Ullah Khan<sup>1</sup> · Manish Patidar<sup>1</sup> · Yuvraj K. Madhukar<sup>1</sup>

Received: 13 November 2021 / Revised: 19 April 2022 / Accepted: 17 August 2022 / Published online: 19 September 2022  
© The Author(s), under exclusive licence to Korean Society for Precision Engineering 2022

## Abstract

An approach has been developed to automate the gas tungsten arc welding (GTAW) process. The process temperature was monitored in-situ and employed to implement feedback control using the infrared ratio pyrometer. The automation of the process was achieved by replacing the foot pedal of the GTAW power source with an in-house developed control system consisting of a data acquisition system and a relay. The GTAW current was made variable automatically to achieve the desired or setpoint temperature. The temperature control is demonstrated for a broad range of 400–1600 °C for both stationary and moving heat source (GTAW torch). The standard deviation from the setpoint temperature was found to be within  $\pm 25$  °C for all the cases. It was also implemented for the single-pass bead deposition by feeding a low alloy steel wire to control the bead temperature in the range of 1200–1400 °C at different deposition speeds. The bead geometrical and mechanical properties could be altered by controlling the deposition temperature. The maximum bead width increased, and height decreased with the increase of the deposition temperature at a constant deposition speed. The microhardness was found to decrease by  $\sim 12\%$  with the increase in deposition temperature from 1200 to 1400 °C, while the deposition speed had a marginal effect.

**Keywords** Temperature control · Feedback control · GTAW · Ratio pyrometer · Automation

## 1 Introduction

Tungsten Inert Gas (TIG) or Gas Tungsten Arc Welding (GTAW) is a traditional method of quality welding. It is useful in many applications due to its capability to execute all three types of welding, namely autogenous, homogeneous and heterogeneous. It refers to the methods when no-filler material, filler same as the base material, and filler different from the base material are utilised. Researchers have widely studied this process for a broad range of materials, including metals and alloys, to explore its advantages and the various process applicabilities [1, 2].

This non-consumable electrode process (GTAW) is utilised extensively in various other applications such as surface hardening [3], melting [4], alloying [5], cladding [6], and additive manufacturing (AM) [7], and many others, due to its cost-effectiveness and ease of handling. Kumar et al. [4] performed surface modification in AISI 4340 steel using

a multi-pass GTAW arcing process. They studied the effect of process parameters by varying the arc current and travel speed while keeping the arc voltage constant at  $10.5 \pm 1.0$  V to control the heat input. They found that the surface hardness improved from 250 to 720 HV. Ulutan et al. [5] utilised the GTAW process for surface alloying. They reported that the alloying of SiC on the steel substrate could vary the surface hardness between 670 and 1165 HV. They also observed a difference between surface and inner part properties with high heat input, which induced residual stresses. Lv et al. [6] compared hot and cold copper wire cladding on the steel substrate. An additional GTAW arc was used for the heating of the wire. They found that below 240 A, the spreadability of hot wire was better than cold wire. The clad hardness improved with the current and dependent on ferrous (Fe) content.

Owing to many applications, the GTAW process needs automation, in-situ monitoring, and control for further industrialization of these applications. The GTAW arc interaction with the work surface results in a melt pool and surrounding thermal concentrated zones. The formed melt pool, its peak temperature and cooling rate could affect the different mechanical and metallurgical properties. It makes melt pool

✉ Yuvraj K. Madhukar  
yuvrajmadhukar@iiti.ac.in

<sup>1</sup> Department of Mechanical Engineering, Indian Institute of Technology Indore, Indore 453552, India

and surrounding thermally concentrated zones an important parameter to monitor and control in-situ. Wei et al. [8] reviewed in-situ monitoring methods for quality control and process stability. They emphasized adopting optoelectronic-based methods such as pyrometer and CMOS/CCD cameras for melt pool monitoring. The pyrometer provides a non-contact solution which is also helpful when the target is not stationary. Single-color and the ratio pyrometer are the two independent technologies to monitor the temperature. However, the effect of emissivity dependence on temperature measurement could be minimized in ratio technology. For surface morphology, digital cameras with specific filters and shielding glass were suggested. This obtained information is then communicated to the real-time closed-loop control system that regulates the process parameters. Gopinath et al. [9] conducted a study on online monitoring of the thermal cycles during the laser cladding process. They correlated temperature variation with different aspects of the material properties such as microstructure, elemental segregations, and others. They found that monitoring the process would prevent overheating, hence less vaporization or material loss. Kejie et al. [10] controlled the welding speed to achieve a stable penetration depth in GTAW welding. They used image processing to measure the penetration and PID (Proportional–Integral–Derivative) controller to control welding speed. Na et al. [11] performed real-time monitoring of arc length and melt pool surface depression in the robotic GTAW process. They used the arc acoustic signal to predict and thus control the arc height within an error of 0.5 mm.

The GTAW has also been used for the additive manufacturing of metallic parts. The GTAW-based wire arc additive manufacturing (WAAM) offers parts free from defects such as porosity, micro cracks, delamination, and oxidation for most metals. Wu et al. [12] reported that online temperature and heat input could be controlled to achieve the desired microstructure and mechanical properties. Williams et al. [13] reported that there are associated limitations to achieve complex geometry and make it defect-free. They also suggested that real-time temperature monitoring and feedback systems could minimize these limitations. Xiong et al. [14] implemented the real-time sensing of the GTAW-based WAAM for stable manufacturing. They controlled the wire feed rate with the help of the PID controller to achieve constant bead height within a range of 0.4 mm. Huang et al. [15] proposed a dynamic control strategy to control the temperature field during the selective laser sintering process. They were able to improve the part quality by increasing the tensile strength by 15.4%.

Based on the available literature, it can be concluded that the GTAW process has a wide range of applications, and many of these applications require controlled heating and melting of the material. The harmful radiation of these welding processes and related health issues caused a significant

reduction in skilled operators in the field needing automation of the process. Further, the applications such as surface hardening, additive manufacturing, cladding, alloying, etc., require trivial control of the deposition parameters as it is taken from the CAD (computer-aided design) model. In this presented experimental work, a simple and easy to adopt method has been developed, enabling the GTAW welding machine to be programmable. A data acquisition system (DAQ) was used to bridge the communication between a computer and a GTAW power source. It was achieved by replacing the foot pedal control of the machine with a DAQ. A feedback control system was implemented, considering the generated temperature as a primary parameter. This feedback control regulates the input power to maintain the desired temperature at the desired location. A wide range of experiments were performed to establish the process, such as temperature control at a different magnitude while keeping the GTAW torch stationary, moving at different speeds and during single bead deposition.

## 2 Materials and Methods

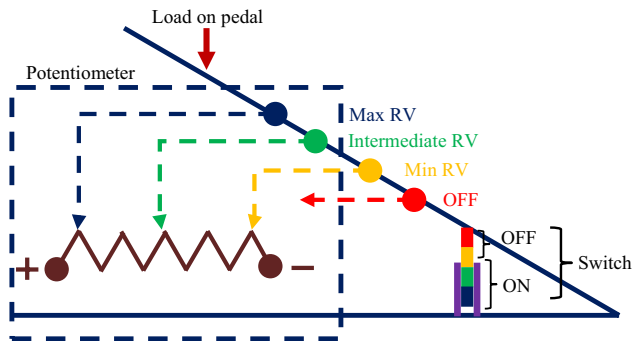
### 2.1 Experimental Details

The experiment was carried out with a 300A GTAW (AC/DC) welding machine (make: kemppi, model: MasterTig MLS 3003ACDC). It was equipped with standard features such as HF (high frequency) start, the remote control using a foot pedal, and manual control to set the arc current. A straight neck air-cooled torch was used. This type of torch is desirable for automated systems for ease of mounting on CNC (Computer Numerical Control) machines. A three-axis CNC gantry was designed and developed in-house for the purpose [16, 17]. The utilised electrode was a 2% thoriated tungsten electrode with a diameter of 2.4 mm. Argon gas was used as an inert gas at a constant flow rate of 10 L/min. All the experiments were conducted on the DC mode of operation, keeping the straight polarity (DCEN-Direct Current Electrode Negative). Stainless steel (SS316) sheet of thickness 1.5 mm and mild steel sheets of 3 mm were used as the substrate for different experiments. The chemical composition of the materials is presented in Table 1. The cross-sections of the deposited beads were observed using the stereomicroscope (Leica EZ4 HD) to measure its width and height. The micro-indentation hardness was measured using a Vickers hardness tester (UHL VMHT). A load of 300 gf was applied for 15 s. The hardness was measured along a vertical line at the center of the beads, and their average was considered for comparison.

A DAQ system (NI USB-6001) was used to bridge the communication between a computer and the GTAW source. It was achieved by replacing the foot pedal control of the

**Table 1** Chemical compositions of the materials used

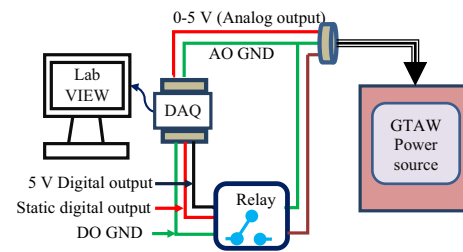
Material	C	Si	Mn	P	S	Cr	Ni	Mo	Cu	N	Fe
Stainless steel (304L)	0.017	0.37	1.79	0.028	0.010	18.1	8	0.4	0.34	0.06	Bal
Mild steel (AISI 1020)	0.18	0.4	0.9	0.04	0.04	–	–	–	–	–	Bal
Low alloy steel (ER70S-6)	0.09	0.9	1.6	0.007	0.007	0.05	0.05	–	0.2	–	Bal

**Fig. 1** Schematic of the construction of foot pedal at different conditions. The various positions of the switch (represented by different colours) show the different positions of the wipers

machine with the DAQ. The LabVIEW software was used for the appropriate programming. The temperature control was introduced after the successful implementation of the programmable control of the GTAW power source. A non-contact two-color (ratio) pyrometer (make: LumaSense Technologies, model: IGAR-6 Advanced) was used to monitor the in-situ temperature. The working wavelengths of the pyrometer were 1500–1600 nm and 2100–2500 nm for channel-1 and channel-2, respectively. It can also be operated in a single-channel mode where radiation from the entire spectrum of both the channels is considered. The minimum response time of the pyrometer is 2 ms, and the working temperature ranges from 250 to 2000 °C in ratio mode and 100 °C to 2000 °C in single-channel mode, respectively. The pyrometer has a visible laser sighting for focusing the target object for temperature measurement with a minimum spot diameter of 2.1 mm at a distance of ~210 mm. This pyrometer could also be communicated through provided ASCII codes [18]. A feedback control system was implemented, taking the temperature as an input parameter.

## 2.2 Enabling Computer Control in GTAW

The basic construction of the GTAW machine allows the user to ignite and control the arc current using the foot pedal. This foot pedal is used to control the GTAW system remotely. Figure 1 shows the schematic construction and the working principle of the foot pedal. It consists of a mechanical switch and a potentiometer. It is positioned inside the pedal in such a way that with an application of load, the

**Fig. 2** Schematic diagram of the GTAW automation

switch would be operated first and then the potentiometer. The switch ON and OFF position enables and disables the foot pedal, respectively. The ON position also enables the inert gas flow, which is required for arc stabilisation. Further continuation of the load mechanically regulates the potentiometer and defines the welding current.

Primarily the foot pedal regulates the reference DC voltage varying in the range of 0–5 V instead of the actual GTAW parameter (current) available at the torch. The ‘0 V’ represents the minimum and ‘5 V’ the maximum set GTAW current, respectively. With the application of the load on the pedal, the potentiometer wiper position changes, which defines the resistance and hence reference voltage. In general, this resistance varies in the range of 0–10 kΩ. When the pedal is at the “No-load” condition, the switch remains at OFF; hence no GTAW operation would take place. When the pedal is just pressed; it enables the switch to the ON position and triggers the inert gas flow. However, in this condition, the wiper position remains at minimum resistance. This minimum resistance sends the signal to the GTAW machine in terms of the reference voltage (usually lower end of 0–5 V), which regulates the GTAW current to its minimum possible magnitude available with the machine. When the pedal is further pressed, the reference voltage would be regulated depending on the load and position of the potentiometer wiper, which would eventually determine the GTAW current available at the torch.

The mechanical work involved in a foot pedal needs automation for precise variation of the reference voltage, or replacing the pedal with an external control circuit could make the system automated. Figure 2 shows the schematic of the circuit, which replaces the foot pedal with a DAQ system to communicate with the machine and also to control it. The analog output (AO) of the DAQ was used as a reference voltage required to control the arc current. The mechanical

switch of the pedal was replaced by a relay and controlled by the digital output (DO) of the DAQ.

It is to be noted that the foot pedal only regulates the manually set maximum GTAW current in the power source. A study was conducted to analyse the variation in the set GTAW current when regulated through the DAQ system. A dedicated program was written to perform this study. The reference voltage was varied, and the obtained GTAW current was noted from the display. 3A is the minimum current required for the utilised GTAW power source to generate an arc. Therefore, the experiments were conducted for five different current ranges, i.e., 3–33, 3–53, 3–73, 3–103 and 3–153 A, and plotted in Fig. 3. Here the reference voltage was varied with an increment of 0.1 V to analyse the variation in the GTAW current. It was observed that the output current increases with an increase of the reference voltage and has a near-linear relation.

### 2.3 Enabling the Pyrometer Data in LabVIEW and Its Validation

#### 2.3.1 Pyrometer Validation: Ratio Temperature Measurement

Figure 4a shows the experimental setup for validation of the pyrometer. It consists of a halogen lamp, a DC power source, a pyrometer integrated with the processing unit, and a computer. The tungsten filament of the lamp (240 W, 24 V) was used as a target sample. A variable DC power supply controlled the heating of the filament. The filament was in a rectangular shape of width 4 mm and length 10 mm. Since the gap between intermediate coils was small, it was treated as a flat surface.

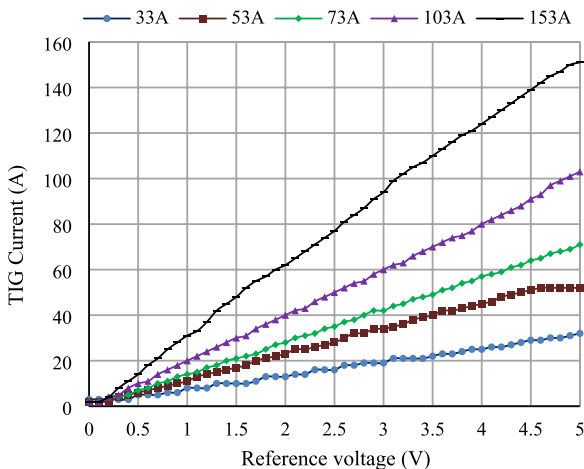
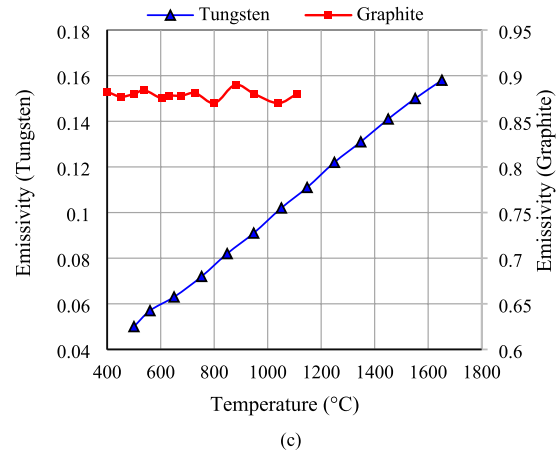
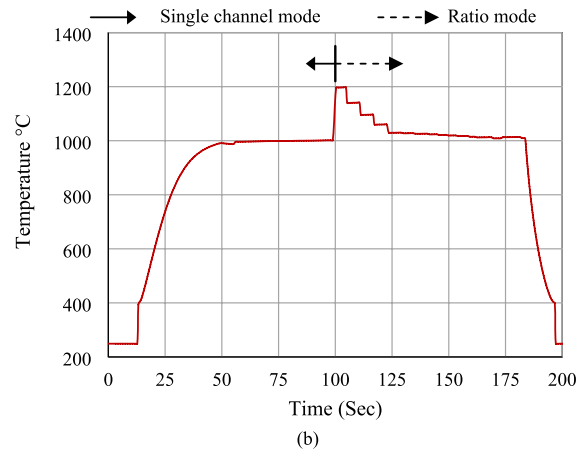
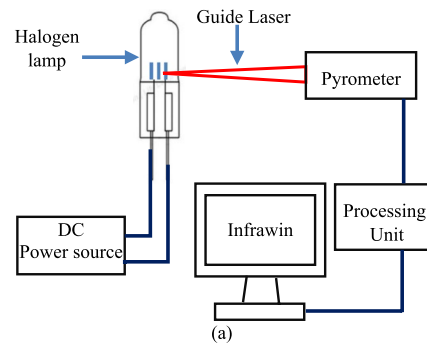


Fig. 3 Variations in GTAW current with reference to the input reference voltage

Fig. 4 Pyrometer validation a schematic, b emissivity measurement through iteration, c variation in emissivity of tungsten and graphite with the temperature

An infrared thermometer measures the temperature by sensing the infrared energy that every material or object radiates above absolute zero Kelvin (0 K). It works on Planck’s law of black body radiation by converting the spectral energy density  $R$  as a function of wavelength  $\lambda$  (m) and temperature  $T$  (K) [19]. The temperature is dependent on the emissivity factor of the heated surface. This dependency on emissivity could be minimized by employing the ratio pyrometer as it takes the radiation from two independent spectra. Therefore,

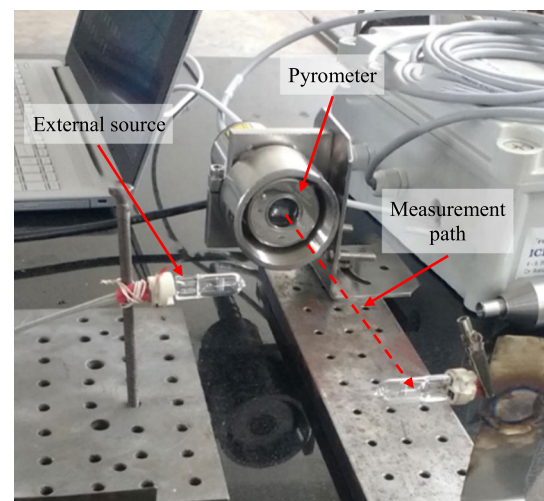
the measured temperature using a ratio pyrometer could be considered more accurate [20]. The utilised pyrometer could be operated in both single-channel and two-channel (ratio) mode. Ideally, the measured body temperature should be identical for both modes. However, in the case of single-channel mode, a known emissivity would be needed. Therefore, the temperature would change depending on the input emissivity value. It could be found that at a specific value of the emissivity for the single-channel mode, the measured temperature would become the same as the ratio mode. The value of this emissivity was obtained here, iteratively, for a stabilised constant temperature (Fig. 4b). The stair steps in Fig. 4b represents the iteration performed to match the temperature. This procedure could be repeated to find the emissivity with respect to temperature for any unknown material. Figure 4c show the found emissivity curve for tungsten filament and graphite sheet. The presented results are matching well with the reported emissivity using different approaches and controlled environment [21, 22].

### 2.3.2 Pyrometer Validation: Effect of External Radiation, Fume, or Dirt

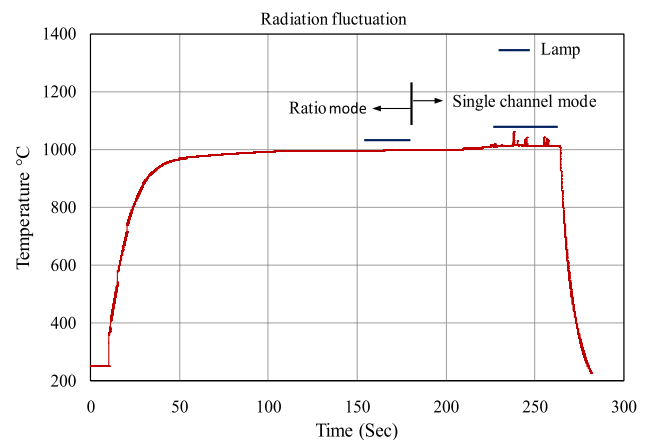
The manufacturing operations are often exposed to external radiation, fumes, and dirt. These circumstances may affect the accuracy of the measured temperature. A series of experiments were performed to study the effects of these factors.

The external radiation may appear in the manufacturing environment from different sources. Therefore, it is essential to analyse and minimise the chances of errors. Both the modes (single channel and ratio mode) of measurement were examined to find the deviation in temperature measurement due to external radiation. An additional lamp was introduced in the measurement path with an offset of about 100 mm (Fig. 5a) for the purpose. The filament temperature was measured in ratio mode first, and the temperature was allowed to stabilise. Then the other lamp was turned-ON. The similar experiment was performed for single-channel mode. From Fig. 5b, it was observed that the ratio mode showed little variation in temperature due to external radiation. The dynamic nature of the temperature signal was observed in the case of the single-channel mode. However, a stainless-steel casing of length 210 mm (focal length of the pyrometer) and an opening of 8 mm was also made in-house to prevent the pyrometer lens from spatters and settling of fumes and dirt.

The presence of the generated fumes, dirt or dust may also reduce the radiation transmission from the measuring site to the pyrometer and result in an error in temperature measurement. Two ND (neutral density) filters were used to simulate a similar effect or block the randomly selected known percentage of the radiation. The chosen



(a)



(b)

**Fig. 5** Effect of external radiation on the temperature measurement **a** experimental setup, **b** time versus temperature reading

ODs (optical density) were 0.1 (80% transmission) and 0.6 (25% transmission), respectively. Here, the temperature was allowed to stabilise at different levels, and then the ND filter was introduced in the measurement path. Figure 6a, b show the recorded temperature behaviour for both the mode of operations while using the ND filters. Figure 6c represents the percentage error for both modes of operations. The error in the ratio mode of operation could be because of variation in transmission for the working wavelength of the pyrometer [23]. It was about 4% and 10% for ND filter of OD 0.1 and 0.6, respectively. This variation would affect the constant emissivity factor in ratio mode, which was reflected in terms of a marginal error. However, the recorded error was lesser in ratio mode compared to the single-channel mode of operation. It makes the ratio pyrometer a good choice for GTAW based applications.

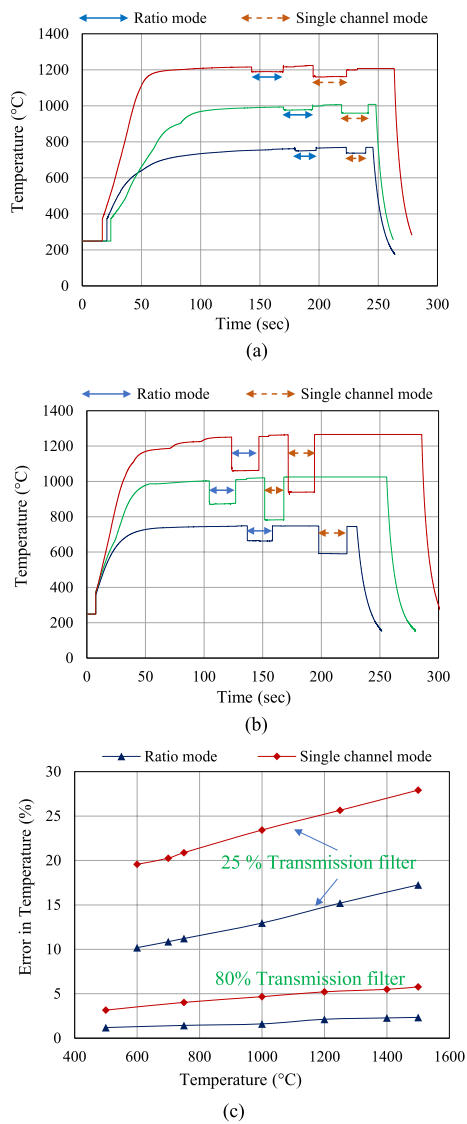


**Fig. 6** Effects of ND filters in temperature measurement at different mode of operation for **a** 0.1 OD (80% transmission), **b** 0.6 OD (25% transmission), **c** percentage error

### 2.3.3 Implementation of the Temperature-Dependent Feedback Control

A dedicated LabVIEW program was written to communicate with the pyrometer bypassing the provided software (Infrawin). The primary objective of this program was to communicate with two hardwares namely, Pyrometer and DAQ I/O. The DAQ device (NI USB-6001) was used for its excellent features such as cost-effectiveness, compactness and multifunctionality. This device is best compatible with the LabVIEW software from national instruments (NI). Therefore, this platform was selected for temperature monitoring and control. The front panel of the developed program is shown in the Fig. 7. The program contains mainly three

parts, i.e., instrument control, in-situ temperature monitoring, and feedback control from the same program. VISA resource name (virtual instrument software architecture) was used to communicate the inputs from the pyrometer using the specified *serial settings* such as *baud rate*, *parity*, *flow control* and others as provided by the manufacturer. ASCII codes were used to access the various temperature monitoring functions of the pyrometer. It was further converted into familiar data in °C. The real time temperature data can be seen by a *waveform chart* and *numeric indicator* on the front panel. *Write to measurement file* tool was used to save the temperature data automatically. The real time data was used as the *process variable* for the inbuilt PID (Proportional–Integral–Derivative) tool. The *numeric control* tool was used for selecting the *setpoint* temperature and *PID gains* on the front panel. For control, gains were optimised for the desired *setpoint* temperature. The PID output range was set to 0–1000 and converted to 0–5 which was utilised as reference voltage communicated through *DAQ analog output channel*. *Boolean TF* button was used to control the inert gas and arc ignition ON/OFF through the *DAQ assistant*. All the palettes after the VISA serial were kept inside a *while*-loop to repeat the code till stopped manually using *boolean TF* button. The generated feedback signal was communicated to the GTAW welding power source using the DAQ to control the arc current and hence the temperature.

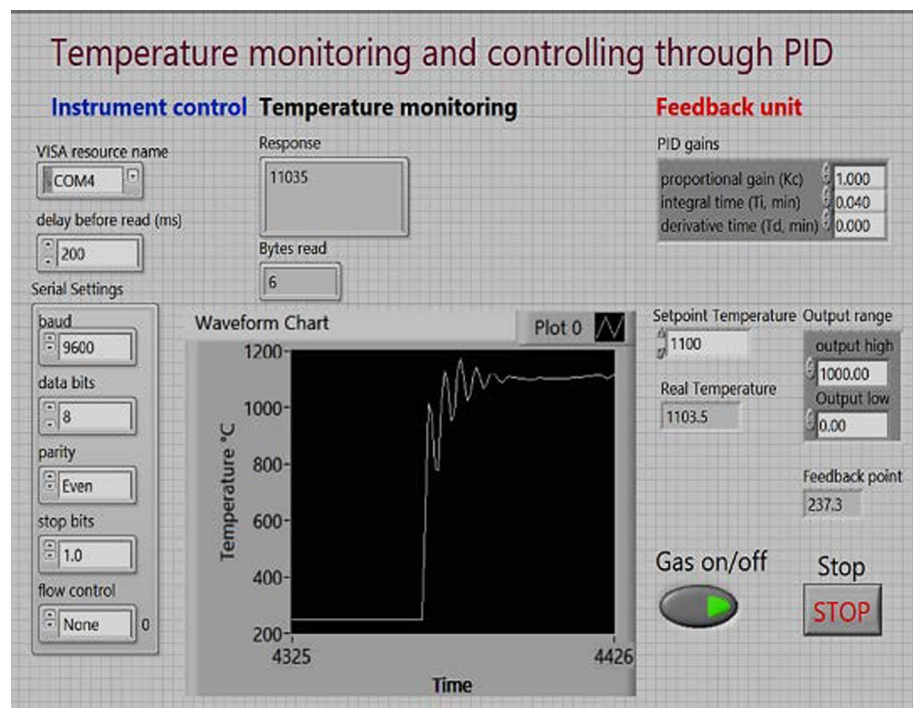
## 3 Results and Discussion

### 3.1 Temperature-Dependent Feedback Control for the Stationary Heating Source

Figure 8a shows the schematic of the experimental setup, where the GTAW torch was kept stationary and targeted to a test sample. Two sets of experiments were performed. In the first set, the pyrometer was focused on the sample, which was in line with the tip of the electrode (Fig. 8b). In the second set of the experiment, the pyrometer was focused offset from the tip of the electrode of about 8 mm (Fig. 8c).

Figure 9 shows the recorded controlled temperature with respect to the time. The setpoint temperature was varied from ~600 to ~1300 °C with an increment and decrement of 100 °C. The setpoint temperature was changed after each ~100 s. It was chosen to allow the GTAW source to stabilise the temperature. The utilised PID constants were found through iteration to achieve the optimum result. It was 1.0, 0.04 and 0.00 for proportional, integral and derivative, respectively. The iteration was performed by increasing the proportional gain ( $K_c$ ) in a step of 0.1 at first, while keeping the integral ( $T_i$ ) and derivative time ( $T_d$ ) zero.  $K_c$  was increased until the desired setpoint temperature was reached or exceeded. It was found to be 1.0 in this case.  $T_i$  was varied

**Fig. 7** Front panel of the developed LabVIEW program



afterward in the steps of 0.01 while keeping  $T_d$  still zero. It was observed that keeping the  $K_c$  at 1 and  $T_i$  at 0.04 stabilised the temperature response efficiently. The variation in  $T_d$  was observed to be resulting in unstable outputs. Therefore, the best condition was found for PI mode of control. These constants were kept unchanged for both the set of experiments.

It was observed that the obtained temperature was in a close range of the desired setpoint for both sets of experiments. In the first set of the experiment (when the pyrometer was focused in line with the electrode), the temperature stabilisation for above 1200 °C and below 700 °C could not be achieved for decremental control. It is because of the proportional constant of the PID, which overshoots the temperature above the melting and causing the piercing of the sample for the setpoint of 1300 °C and above. However, in the case of below 700 °C, the heat dissipation drops as the bulk temperature increased due to a decremental change in the setpoint temperature. A similar effect was observed in the case of the second set of the experiment (the pyrometer was focused offset with the electrode); the stabilisation in temperature above 1100 °C could not be achieved for both incremental and decremental control. However, decreasing setpoint temperature of up to 500 °C was achieved successfully. The standard deviation was found to be in the range of  $\pm 16$  °C and  $\pm 06$  °C, respectively, for in-line and offset-focused temperature control. This deviation was found to remain almost constant for both increasing and decreasing temperature control. The marginal higher deviation in the case of in-line focused control could be because of voltage

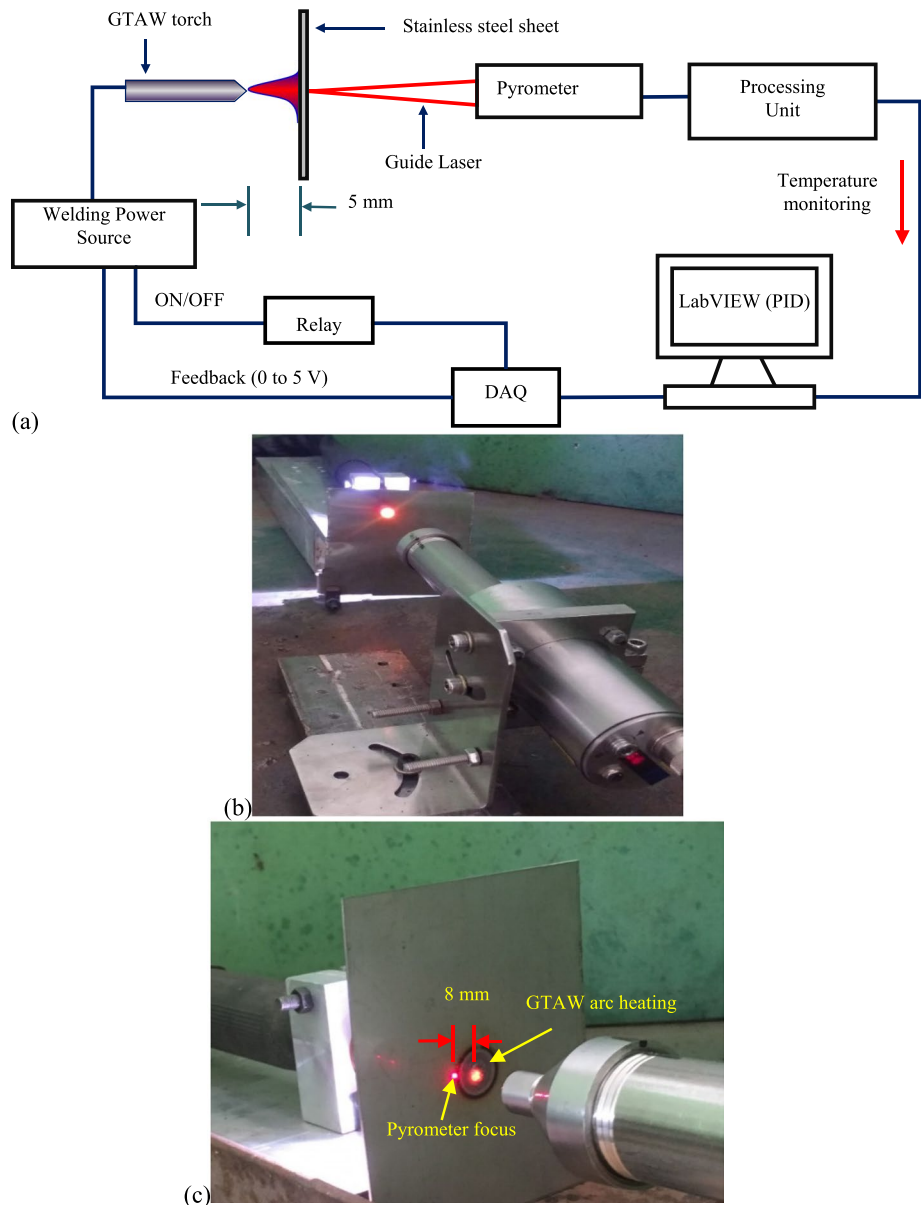
instability in the sustained arc column. This instability in voltage could be considered as an inherent property of the process which exists despite keeping all the parameters (stand-off-distance (SOD), gas flow rate, current) constant [24].

### 3.2 Temperature-Dependent Feedback Control for the Moving Heating Source

Figure 10a shows the schematic of the experimental setup for the temperature-dependent feedback control for the moving heat source. An in-house developed three-axis gantry CNC was used for the purpose. The GTAW torch and the pyrometer were mounted on the Z-axis, and the heating sample was mounted on the XY motion plate, as shown in Fig. 10b. It makes the torch and pyrometer stationary, which minimizes the chances for errors due to vibration. The pyrometer was focused at a distance of 12 mm behind the arc to achieve the offset, focusing on minimizing the error in controlled temperature as found in the previous set of experiment. However, it was ensured that it always follows the heating seam. The feedback control was implemented for single track heating for different temperatures. The scan speed and SOD were constant throughout the experiment at 60 mm/min and 4 mm, respectively. The PID constants were kept the same as the previous set of experiment.

Figure 11 shows the recorded controlled temperature with respect to the time. The setpoint temperature was varied in three different ways between 1000 to 1600 °C to examine the stability in its control. First, incremental

**Fig. 8** **a** Schematic of the experimental setup for the stationary heat source, pictorial view when the pyrometer was focused, **b** in-line and **c** at an offset of 8 mm with the electrode



only (1000–1100–1200–1300–1400 °C), second decremental–incremental–decremental (1200–1100–1000–1400–1300–1200 °C), and third incremental–decremental (1400–1500–1600–1500–1400 °C). It was observed that the temperature was in a close range to the setpoint temperature for all the sets of the conducted experiment. In all three cases, the standard deviation in controlled temperature was found to be in the range of  $\pm 15$  °C. The broad range of temperature control for surface heating may find many applications in industries such as surface modification, hardening, melting, and many more.

### 3.3 Temperature-Dependent Feedback Control for the Single Bead Deposition

The schematic and experimental arrangement for the temperature-dependent feedback control during single bead deposition is presented in Fig. 12a, b, respectively. A 0.8 mm diameter steel wire (ER70S-6) was fed into the stabilised arc of GTAW using a cold wire feeder (make: ATE welding). Front feeding (as shown in Fig. 12a, b) was adopted and maintained constant throughout the experiment at a constant feed speed of 150 mm/min. The pyrometer was focused on the



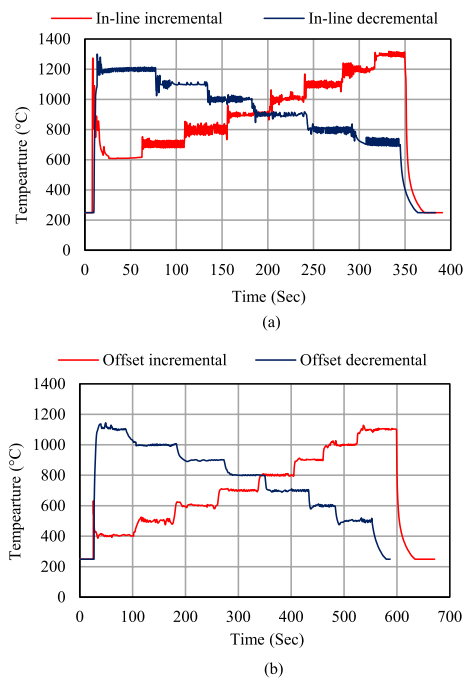


**Fig. 9** The incremental and decremental controlled temperature with respect to the time when the pyrometer was focused **a** in-line, and **b** at an offset of 8 mm with the electrode

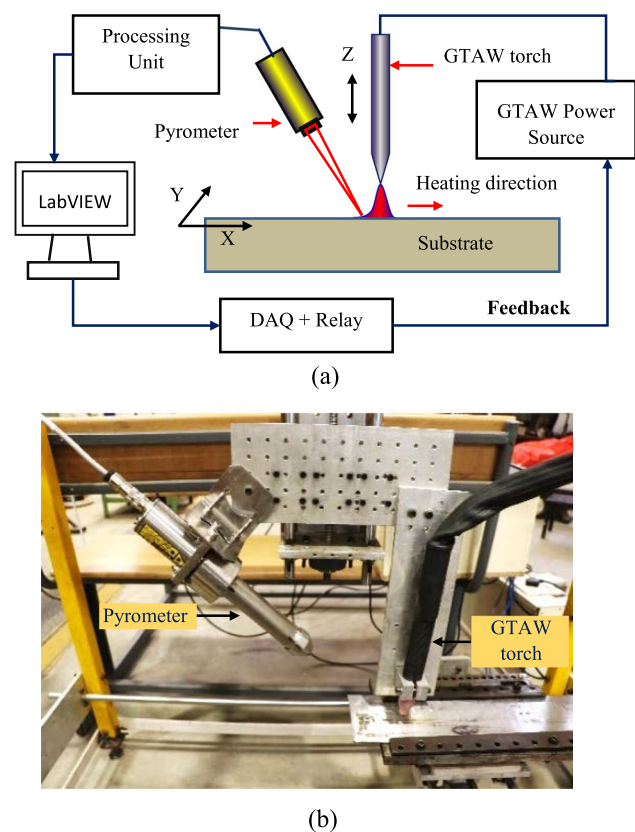


**Fig. 10** **a** Schematic and **b** experimental arrangement for moving heat source temperature control

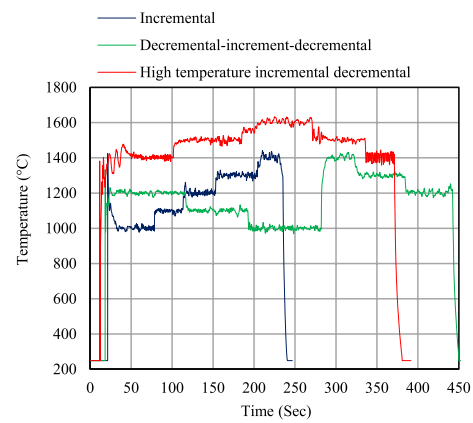


**Fig. 11** The Feedback temperature control for the moving heat source for incremental, decremental–increment–decremental, and high range temperature control for both incremental and decremental

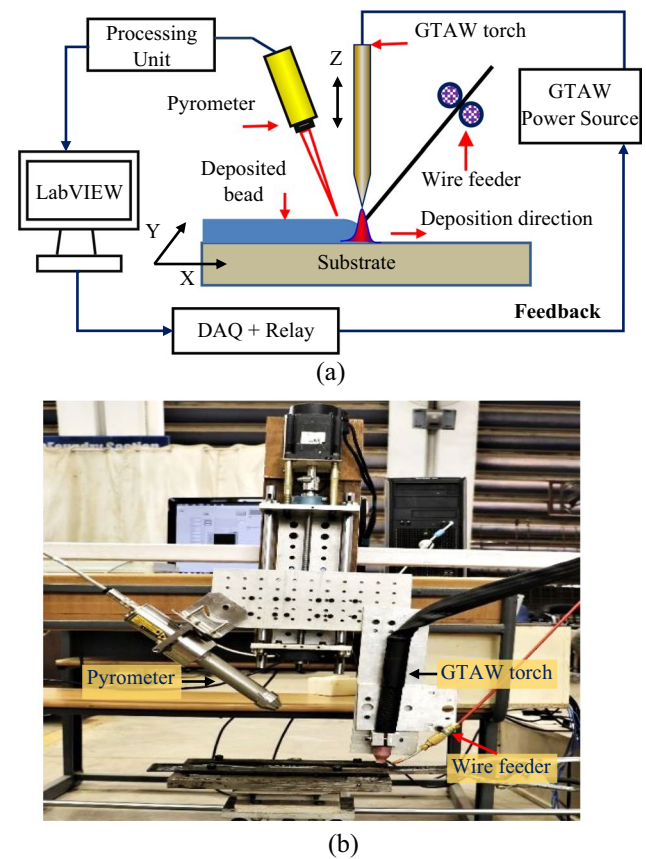


**Fig. 12** **a** Schematic and **b** experimental arrangement for deposition of single bead temperature control

deposited bead at a distance of 12 mm behind the arc. It was kept at a near-vertical position behind the arc to maximize the gain (radiation), which would be relatively scattered due to curved bead profile and striations. The experiment was performed at four different deposition speeds, which are 150,

200, 250 and 300 mm/min. The deposition speed range was optimised based on trial experiments to obtain the continuous and uniform bead. It was observed that the reduction of deposition speed below 150 mm/min caused overheating of the wire and the base plate, causing non-uniform bead formation, whereas exceeding the speed above 300 mm/min leads to discontinuous deposition.

The single bead deposition temperature control was performed for three setpoint temperatures, i.e. 1200 °C, 1300 °C and 1400 °C for each deposition speed. Figure 13 shows the recorded controlled temperature during the deposition. The experiments were also extended to change the setpoint temperature during a single track deposition. Figure 14 shows the single track feedback temperature control for both increasing trends (1200 °C to 1400 °C) and the decreasing trend (1400–1200 °C). It was observed that in all the cases, the bead temperature remains in close range to the setpoint temperature. In all four cases, the standard deviation in controlled temperature was found to be within  $\pm 25$  °C. This error was marginally higher than in the previous cases. The temperature was observed taking a relatively long time to stabilise (about 20–25 s). However, it also includes the time required for any particular point of deposition to reach the measurement point, 12 mm behind. This required time varies in the range of 2.4–4.8 s, depending on the deposition speed. During this time, the pyrometer receives radiation only from the conducted heat as it was placed behind the arc. It could also be the reason for the high fluctuation in measured temperature at the beginning. The bead deposition is a dynamic process, which involves heating, melting and again solidification of the material. This transition from liquid to solid and further cooling leads to variation in surface emissivity [25]. If emissivity varies temporally and by the same amount at both pyrometer wavebands, then it should not affect the temperature measurement. However, if the emissivity varies differently in the two wavebands, the accuracy of the temperature measurement would be affected [20]. This variation becomes significant when the cooling occurs at a fast rate, e.g. in the present study ( $\sim 20$  s to reach a temperature of  $\sim 250$  °C), Fig. 13. It would lead to scattered temperature data. The PID uses this data for the calculation of reference voltage. Hence, a long time would be required for PID to respond and find the optimum reference voltage, which eventually would become scattered. Since the utilised GTAW power source could not be able to cope up with a very small change in current (resolution 1 Amp), the power would remain constant. Hence, the bead temperature would remain in its trend (either increasing or decreasing) for a longer duration, resulting in a marginal increase in error.

Figure 15a shows the cross-sections of the deposited beads. It was observed that the bead geometry (maximum width and height) has a direct relation with deposition temperature. For a constant deposition speed, the effective

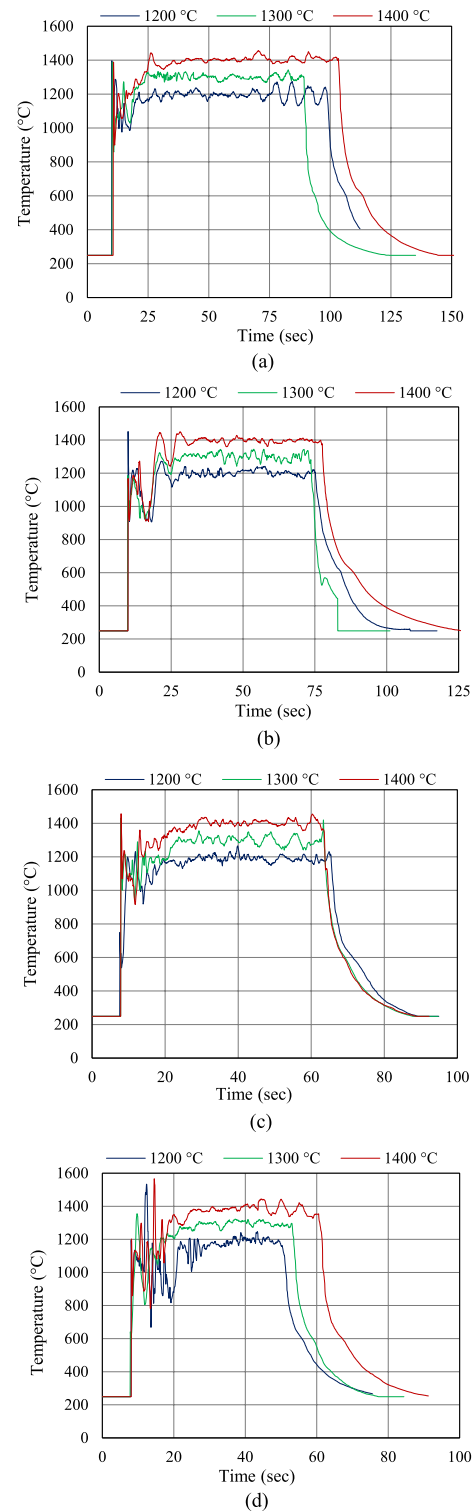


**Fig. 13** Temperature-dependent feedback control for the single bead deposition with the moving heat source at different travel speed **a** 150 mm/min, **b** 200 mm/min, **c** 250 mm/min, **d** 300 mm/min, for different temperatures

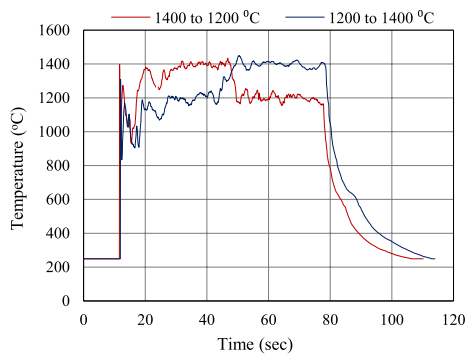
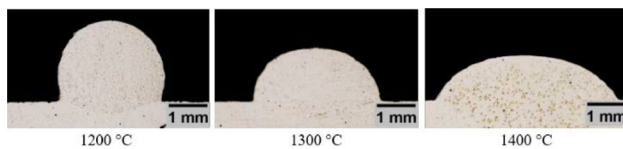
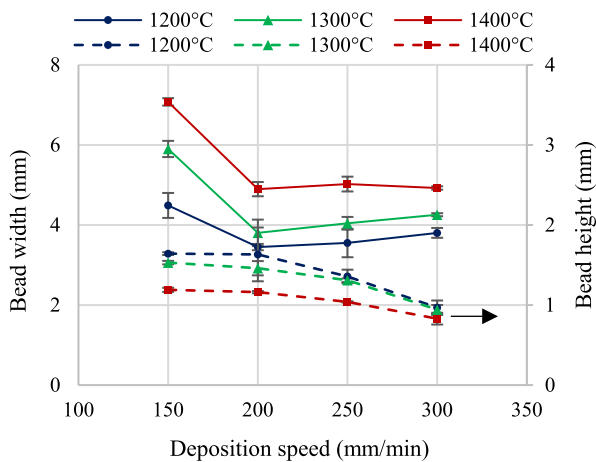


**Fig. 14** Singletrack deposition, multiple temperature control at 150 mm/min deposition speed



(a)



(b)

**Fig. 15** Bead geometry variation, **a** typical bead geometry variation with different setpoint temperature, and variation of bead, **b** width (continuous lines) and height (dashed lines) with deposition temperature at different setpoint temperatures

bead width increased, and the bead height decreased with the increase of the deposition temperature (Fig. 15b). The reason could be the high solidification time resulting from high input energy at the higher setpoint temperature. Hence, the molten metal would flow in the lateral direction till the commencing of solidification. The deposition speeds also affected the bead geometry (Fig. 15b). Both bead width and height were found to decrease with the deposition speed. However, the bead width showed marginal variation at higher speeds.

**Table 2** Performance evaluation parameters for different setpoint temperatures at different travel speeds

Travel speed (mm/min)	Setpoint temperature (°C)		1200				1300				1400					
	Rise time (s)	Overshoot %	Stabilisation time (s)	Steady-state error %	Rise time (s)	Overshoot %	Stabilisation time (s)	Steady-state error %	Rise time (s)	Overshoot %	Stabilisation time (s)	Steady-state error %	Rise time (s)	Overshoot %	Stabilisation time (s)	Steady-state error %
150	11.20	6.25	16.98	0.55	13.78	3.31	14.02	0.79	14.82	4.03	30.29	0.42	14.82	4.03	30.29	0.42
200	10.06	6.03	20.22	0.96	10.61	3.43	15.15	1.21	9.49	3.5	23.39	0.73	9.49	3.5	23.39	0.73
250	21.30	5.42	22.59	1.22	15.40	4.29	16.35	1.02	21.08	4.05	24.79	0.68	21.08	4.05	24.79	0.68
300	16.32	3.90	23.10	1.08	19.23	1.73	19.81	0.88	22.42	3.13	27.18	0.77	22.42	3.13	27.18	0.77

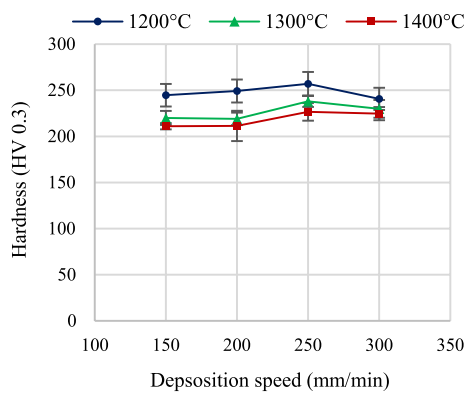


**Fig. 16** Micro-indentation hardness of the deposited beads

Performance parameters to validate the effectiveness of the control system were also analysed and presented in Table 2. It includes the rise time (time taken to reach the specified setpoint), overshoot percentage (percentage of temperature exceeding the setpoint), stabilisation time (time taken to reach stability/zone of acceptable error), and steady-state error percent (percentage of average deviation between setpoint and the controlled temperature in the stable regime). The stabilisation time was ranging from ~ 14 to 30 s. Once it reaches the stability, the steady-state error was insignificant ranging from ~ 0.4–1.2%. The overshoot at the beginning was lying in the range of ~ 1.7–6%, which was stabilised quickly.

Micro-indentation hardness measurement was performed to analyse the effects of different setpoint temperatures on the deposited beads. Figure 16 shows the variation of hardness with the increase of deposition speed at different setpoint temperatures. The represented hardness was the average of five indents on the bead cross-section along with its height. It was observed that the higher setpoint temperatures led to lesser hardness and vice-versa, while the deposition speed had a marginal effect. The lower heat input in the case of the low setpoint temperature results in a high cooling rate which increases the material hardness [26]. As the heat input increases, the hardness of the material keeps decreasing. In general, the low heat input deposited beads are undesirable due to their tendency to crack, high hardness and poor toughness [27]. It makes the beads deposited at 1400 °C more favorable for part deposition concerning the mechanical properties. Since the deposition speed has little effect on hardness, the deposition speed could be varied during the deposition to achieve the desired bead geometry. The found results would be helpful for the deposition in regions such as joints and corners where bead size could be reduced to prevent the accumulation of material. In this way, the controlled temperature could be used to ensure uniform part quality.

## 4 Conclusions

The objective of the present experimental investigation was to in-situ monitor and control the generated temperature during GTAW application. A control system was developed in-house to replace the foot pedal control of the GTAW power source for the successful implementation of the programmable control. It was observed that the use of a ratio pyrometer would be an appropriate selection for temperature monitoring as it has a little measurement error. It significantly minimizes the effect of external factors such as external radiation, fumes, dirt, and change in emissivity. It makes it very useful in on-floor manufacturing applications where precise control in the environment would not be possible, as demonstrated in this study. The developed in-situ temperature monitoring and PID-based feedback control worked satisfactorily for a broad range of temperature control between 400 and 1600 °C. It was also examined in different experimental conditions such as stationary heating source while monitoring the temperature in-line and offset, moving heat source at a different speed and bead deposition for additive manufacturing. It was observed that for stationary heating, the setpoint temperature could be attained in relatively less time as compared to the moving heat source. A single bead was deposited successfully at a controlled temperature between 1200 and 1400 °C at different deposition speeds. The error in controlled temperature was found in between 0.3 and 1.67% (5–25 °C) in different experimental conditions, whereas the maximum error was realized for the dynamic heat source and bead deposition temperature control 1–1.67% (15–25 °C). It was found that the deposited bead properties such as height, width, and hardness could be controlled by controlling the deposition temperature. The developed system would also be equally useful for other GTAW based applications such as surface hardening, cladding, surface melting, alloying, etc.

**Acknowledgements** The authors would like to thank the technical staff of Central Workshop IIT Indore for their consistent help and support. They also thank Dr Satyajit Chatterjee for allowing to access the Tribology Laboratory facilities. Extended help from the Department of Mechanical Engineering, IIT Indore, is gratefully acknowledged.

**Funding** This work was supported by the Science and Engineering Research Board, India [CRG/2020/001068] under the CRG scheme.

## References

- Balasubramanian, M., Jayabalan, V., & Balasubramanian, V. (2009). Effect of pulsed current gas tungsten arc welding parameters on microstructure of titanium alloy welds. *Journal of Manufacturing Science and Engineering, Transactions of the ASME*, 131(6), 0645021–0645024. <https://doi.org/10.1115/1.4000373>

2. Norman, A. F., Drazhner, V., & Prangnell, P. B. (1999). Effect of welding parameters on the solidification microstructure of autogenous TIG welds in an Al–Cu–Mg–Mn alloy. *Materials Science and Engineering A*, 259(1), 53–64. [https://doi.org/10.1016/S0921-5093\(98\)00873-9](https://doi.org/10.1016/S0921-5093(98)00873-9)
3. Keshavarz, M. K., Gontcharov, A., Lowden, P., & Brochu, M. (2020). A Comparison of weldability, structure, and mechanical properties of CM64 and Tribaloy T-800 welds for hard-facing of turbine blades. *Journal of Manufacturing Science and Engineering*, 142(10), 101004. <https://doi.org/10.1115/1.4047142>
4. Kumar, S., Ghosh, P. K., & Kumar, R. (2017). Surface modification of AISI 4340 steel by multi-pass TIG arcing process. *Journal of Materials Processing Technology*, 249(March), 394–406. <https://doi.org/10.1016/j.jmatprotec.2017.06.035>
5. Ulutan, M., Yildirim, M. M., Buytoz, S., & Çelik, O. N. (2011). Microstructure and wear behavior of TIG surface-alloyed AISI 4140 steel. *Tribology Transactions*, 54(1), 67–79. <https://doi.org/10.1080/10402004.2010.519859>
6. Lv, S. X., Xu, Z. W., Wang, H. T., & Yang, S. Q. (2008). Investigation on TIG cladding of copper alloy on steel plate. *Science and Technology of Welding and Joining*, 13(1), 10–16. <https://doi.org/10.1179/174329307X249414>
7. Panchagnula, J. S., & Simhambhatla, S. (2018). Manufacture of complex thin-walled metallic objects using weld-deposition based additive manufacturing. *Robotics and Computer-Integrated Manufacturing*, 49(June), 194–203. <https://doi.org/10.1016/j.rcim.2017.06.003>
8. He, W., Shi, W., Li, J., & Xie, H. (2019). In-situ monitoring and deformation characterization by optical techniques; part I: Laser-aided direct metal deposition for additive manufacturing. *Optics and Lasers in Engineering*, 122(June), 74–88. <https://doi.org/10.1016/j.optlaseng.2019.05.020>
9. Muvvala, G., Patra Karmakar, D., & Nath, A. K. (2017). Online monitoring of thermo-cycles and its correlation with microstructure in laser cladding of nickel based super alloy. *Optics and Lasers in Engineering*, 88, 139–152. <https://doi.org/10.1016/j.optlaseng.2016.08.005>
10. Kejie, D., Wentan, J., Jincheng, W., & Fujun, Z. (2010). The Research of Adaptive PID for the Thin-Walled Cylinder TIG Welding Penetration Control. In *2010 international conference on computing, control and industrial engineering* (pp. 30–33). <https://doi.org/10.1109/CCIE.2010.15>
11. Lv, N., Zhong, J., Chen, H., Lin, T., & Chen, S. (2014). Real-time control of welding penetration during robotic GTAW dynamical process by audio sensing of arc length. *The International Journal of Advanced Manufacturing Technology*, 74(1–4), 235–249. <https://doi.org/10.1007/s00170-014-5875-7>
12. Wu, B., Pan, Z., Ding, D., Cuiuri, D., Li, H., Xu, J., & Norrish, J. (2018). A review of the wire arc additive manufacturing of metals: Properties, defects and quality improvement. *Journal of Manufacturing Processes*, 35(February), 127–139. <https://doi.org/10.1016/j.jmapro.2018.08.001>
13. Williams, S. W., Martina, F., Addison, A. C., Ding, J., Pardal, G., & Colegrove, P. (2016). Wire + arc additive manufacturing. *Materials Science and Technology*, 32(7), 641–647. <https://doi.org/10.1179/1743284715Y.0000000073>
14. Xiong, J., & Zhang, G. (2014). Adaptive control of deposited height in GMAW-based layer additive manufacturing. *Journal of Materials Processing Technology*, 214(4), 962–968. <https://doi.org/10.1016/j.jmatprotec.2013.11.014>
15. Huang, X. K., Tian, X. Y., Zhong, Q., He, S. W., Huo, C. B., Cao, Y., Tong, Z. Q., & Li, D. C. (2020). Real-time process control of powder bed fusion by monitoring dynamic temperature field. *Advances in Manufacturing*, 8(3), 380–391. <https://doi.org/10.1007/s40436-020-00317-y>
16. Khan, A. U., & Madhukar, Y. K. (2020). An economic design and development of the wire arc additive manufacturing setup. *Procedia CIRP*, 91, 182–187. <https://doi.org/10.1016/j.procir.2020.02.166>
17. Khan, A., & Madhukar, Y. K. (2021). Effects of pillar-based substrate on the wire arc additive manufacturing process. *International Journal of Precision Engineering and Manufacturing*. <https://doi.org/10.1007/s12541-021-00529-7>
18. IMPAC Pyrometers IGAR 6 Advanced manual. LumaSense Technologies. <https://www.advancedenergy.com/globalassets/resources-root/manuals/en-op-igar-6-advanced-manual.pdf>
19. Zohuri, B. (2018). Cryogenic technologies. *Physics of Cryogenics*. <https://doi.org/10.1016/b978-0-12-814519-7.00001-x>
20. Müller, B., & Renz, U. (2001). Development of a fast fiber-optic two-color pyrometer for the temperature measurement of surfaces with varying emissivities. *Review of Scientific Instruments*, 72(8), 3366–3374. <https://doi.org/10.1063/1.1384448>
21. Verret, D. P., & Ramanathan, K. G. (1978). Total Hemispherical Emissivity of Tungsten. *Journal of the Optical Society of America*, 68(9), 1167–1172. <https://doi.org/10.1364/JOSA.68.001167>
22. Wang, H., Chen, D., Wang, G., Long, Y., Luo, J., Liu, L., & Yang, Q. (2013). Measurement technology for material emissivity under high temperature dynamic heating conditions. *Measurement: Journal of the International Measurement Confederation*, 46(10), 4023–4031. <https://doi.org/10.1016/j.measurement.2013.07.041>
23. NENIR501B Ø1/2' Unmounted NIR Absorptive ND Filter, OD: 0.1. (2021). Thorlabs. [www.thorlabs.com/thorproduct.cfm?partnumber=NENIR501B](http://www.thorlabs.com/thorproduct.cfm?partnumber=NENIR501B).
24. Uhrlandt, D., Baeva, M., Pipa, A. V., Kozakov, R., & Gött, G. (2014). Cathode fall voltage of TIG arcs from a non-equilibrium arc model. *Welding in the World*, 59(1), 127–135. <https://doi.org/10.1007/s40194-014-0188-x>
25. Yan, Z., Liu, W., Tang, Z., Liu, X., Zhang, N., Li, M., & Zhang, H. (2018). Review on thermal analysis in laser-based additive manufacturing. *Optics and Laser Technology*, 106, 427–441. <https://doi.org/10.1016/j.optlastec.2018.04.034>
26. Suryana, Pramono, A., Muda, I., & Setiawan, A. (2019). The influence of heat input to mechanical properties and microstructures of API 5L–X65 steel using submerged arc welding process. *MATEC Web of Conferences*, 269, 01009. <https://doi.org/10.1051/matec/conf/201926901009>
27. EuropeanStandards. (2000). Welding recommendations for welding of metallic materials—Part 2: Arc welding of ferritic steels. *Ds/En 1011-2*, 3(1), 26.

**Publisher's Note** Springer Nature remains neutral with regard to jurisdictional claims in published maps and institutional affiliations.

Springer Nature or its licensor holds exclusive rights to this article under a publishing agreement with the author(s) or other rightsholder(s); author self-archiving of the accepted manuscript version of this article is solely governed by the terms of such publishing agreement and applicable law.



**Anas Ullah Khan** is a PhD scholar in the Department of Mechanical Engineering of IIT Indore, India. He is working in the area of wire arc additive manufacturing. He obtained an M.E. degree in CAD/CAM/CAE in 2018 from SGSITS Indore, India and B.Tech in Mechanical Engineering from JUET Guna, India, in 2016. He has co-authored several papers in the area of wire arc additive manufacturing and its control.



**Manish Patidar** is working as a Junior officer at NMDC Limited, India. He received MTech. degree in Production and Industrial Engineering in 2020 from IIT Indore and B.E. degree in

Mechanical Engineering from CDGI Indore in 2017. His master's dissertation is focused on real time temperature monitoring and control of additive manufacturing process. His research interests lie in the fields of additive manufacturing.



**Dr Yuvraj K Madhukar** is an Assistant Professor in the Department of Mechanical Engineering, IIT Indore. He received his PhD from IIT Kharagpur in 2016. He was a Research Associate during 2015–2017 at Heriot-Watt University, Edinburg, U.K. His area of research includes water-assisted laser material processing, wire arc additive manufacturing and its control. He has co-authored several journal and conference papers and a book chapter.